Alarm for Autonomous UAV Radiation Mapping Algorithm

by

Justin Knoll
B.S., United States Military Academy (2020)

Submitted to the Department of Nuclear Science and Engineering
in partial fulfillment of the requirements for the degree of
Master of Science in Nuclear Science and Engineering
at the
MASSACHUSETTS INSTITUTE OF TECHNOLOGY
May 2022

Author .....
Department of Nuclear Science and Engineering, and Draper Scholar
May 13, 2022

Certified by .....
Areg Danagoulian
Associate Professor of Nuclear Science and Engineering
Thesis Supervisor

Certified by .....
Won Kim
Nuclear Engineer, The Charles Stark Draper Laboratory, Inc.
Thesis Reader

Accepted by .....
Ju Li
Battelle Energy Alliance Professor of Nuclear Science and Engineering
and Professor of Materials Science and Engineering, Chair, Department
Committee on Graduate Students

Alarm for Autonomous UAV Radiation Mapping Algorithm

by

Justin Knoll

Submitted to the Department of Nuclear Science and Engineering
on May 13, 2022, in partial fulfillment of the
requirements for the degree of
Master of Science in Nuclear Science and Engineering

Abstract

The purpose of this research is to create an alarm threshold algorithm for use in an autonomous unmanned aerial vehicle (UAV) for radiation mapping purposes in the event of a nuclear disaster or use of nuclear weapons. Information from this alarm could feed into real time decision making on the UAV system, so the alarm is based on data from 1 second collection windows. All data collection was done with a $Cs_2LiLa(Br,Cl)_6$ detector. The testing included both laboratory experiments and full scale flight testing with the UAV system. Several alarm methods were devised and tested, attempting to take advantage of assumptions about the isotopes that would be present in a nuclear disaster and the known properties and gamma ray energies of these isotopes. Most data collection used either ^{137}Cs or ^{60}Co sources. Receiver operating characteristic (ROC) curve analysis demonstrated that alarm methods setting a threshold on narrower energy bins were less sensitive than methods using the full spectrum count rate, while the most sensitive method was to use bins containing all spectrum data up to the full peak energy of the isotopes of interest but ignoring higher energies. Similar ROC curve results were found with a simulated ^{131}I source, indicating this method would also work with other isotopes. This method was then testing with lab and flight test data using a three standard deviation threshold. The median false alarm rate in the background flights was 0.19%, and sources could be successfully detected at high rates from relatively long distances. For example in one flight a 90% detection probability was attained for an 8 mCi cesium source from a total distance of 22±2 m. The probabilities of finding anomalous sources of radiation and false alarm appear to be sufficient based on the observed data, and this method had the best performing ROC curve of those tested.

Thesis Supervisor: Areg Danagoulian
Title: Associate Professor of Nuclear Science and Engineering

Thesis Reader: Won Kim
Title: Nuclear Engineer, The Charles Stark Draper Laboratory, Inc.

Acknowledgments

I would like to thank Radiation Monitoring Devices Inc., including Andrey Gueorgiev and others, for making the E2MKU detector used in this project and their help and expertise in using the detector. I would also like to thank Sandia National Labs and Lee Harding for the use of GADRAS during my research, and the help with using it. I would also like to thank JPEO CBRND for their support of The Charles Stark Draper Laboratory, Inc. CSIRP project which much of the data comes from. I would also like to thank The Charles Stark Draper Laboratory, Inc. CSIRP team, especially Won Kim, Sam Zarovy, Peter Horak, and Rick Baruffi, whose expertise and work on the CSIRP project were very helpful for my research. I also thank my research group at MIT, who gave helpful feedback as I was reporting the progress on my research. The views and conclusions contained herein are those of the author and should not be interpreted as necessarily representing the official policies or endorsements, either expressed or implied, of the U.S. Government.

Contents

1 Introduction **13**

1.1 Radiation Mapping 14

1.1.1 UAV Radiation Mapping 15

1.2 Background Radiation 16

1.2.1 Radiation Sources of Interest 16

1.3 Radiation Detection 17

1.3.1 CLLBC Detector 17

1.3.2 Counting Statistics 18

1.3.3 GADRAS 21

2 Methods **23**

2.1 Data Collection 23

2.1.1 Background Measurements 23

2.1.2 Laboratory Experimentation 26

2.1.3 Flight Testing 27

2.2 Data Analysis 28

2.2.1 Chi Squared Test For Poisson Distribution 28

2.2.2 Spectra Data and Plotting 28

2.2.3 ROC Curves 29

2.2.4 Energy Bin and Alarm Methodology 30

2.3 Computed Spectra 34

3 Results **37**

3.1 Chi Squared Test Results 37

3.2 Bin Analysis and Alarm Results 38

3.2.1 ROC Curves 38

3.2.2 Type I Error Rates 41

3.2.3 Distance from Source of Alarm 44

3.3 Computed Spectra Results 46

4 Conclusions **49**

List of Figures

1-1 Aerial UAV Radiation Mapping. Including a mapping mission with 2 UAVs searchign an area over 1 km away (left). The other is a smaller scale mapping test at Briggs Field at MIT in which the contour pattern is more easily visible (right). Both using real radiation sources of 7.8 mCi ^{137}Cs (right) and a mixed source totalling approximately 98 mCi of mostly ^{60}Co (left). 16

2-1 Maps of the routes taken through Cambridge and Boston for the background radiation measurements. In order from the 9/14/2021 measurement (top) to the 9/20/2021 measurement (bottom). 25

2-2 Energy spectrum displaying the division of the spectrum into 8 bins, the alternating red and blue regions are the bins. This spectrum data comes from a 30 minute measurement of a 3.46 µCi ^{137}Cs source at a distance of 18.7 cm. 31

2-3 Energy spectrum displaying the 2 full peak energy bin setup, the red region is the cesium bin and the orange is the cobalt bin. The spectrum data on the top comes from a flight test with 26 mCi and 8 mCi ^{137}Cs sources, the spectrum on the bottom comes from a flight test with a 85 mCi ^{60}Co. Both flights were at an altitude of 10 m. 32

2-4 Energy spectrum displaying the energy bins from 0 to the full energy peak, the red region is the bin. The top graph displays the cesium bin in red and the second displays the cobalt bin in orange. The spectrum data on the top comes from a flight test with 26 mCi and 8 mCi ^{137}Cs sources, the spectrum on the bottom comes from a flight test with a 85 mCi ^{60}Co. Both flights were at an altitude of 10 m. 33

3-1 ROC curves for all of the alarm methods attempted, and the hypothetical random line for reference. The top ROC curve uses data collected 76.4 cm from a 3.46 µCi ^{137}Cs source. The curve on the bottom was measured 17.9 cm from a 0.14 µCi ^{60}Co source. 39

3-2 ROC curves created from flight test data, only the full spectrum, and 2 bin methods were plotted. The ROC curve uses data collected from a flight at 25 m altitude with several sources placed together totalling approximately 98 mCi of mostly ^{60}Co. The curve was made with data selected to be approximately 110 m from the source. 40

3-3 Spectra plots with background subtracted for real experimental (top) and computed (bottom) data. Both spectra are approximately 30 min at 31 cm from a 3.46 µCi ^{137}Cs source. Count rates above background and live time for the measurements are in the plots, the y axes are different scales because the simulated data has a much higher 662 keV peak. 47

3-4 ROC curves created from computed data in GADRAS, only the full spectrum, full energy peak bin, and Compton continuum and full energy peak bin were included. The data was simulated as 10 m from a 100 µCi ^{131}I source. 48

List of Tables

3.1 Results of the Chi-squared test for a Poisson distribution for the the background measurements collected across the Cambridge-Boston area, listed by date of collection. Maps of the corresponding routes can be found in figure 2-1. P values below 0.00001 are rounded to 0. 38

3.2 Results of the Chi-squared test for a Poisson distribution for various background flights. P values below 0.00001 are rounded to 0. 38

3.3 Statistical analysis summary for the counts found in each energy bin for the UAV flights measuring background at various locations. The background data from Utah was not a dedicated background flight, but data selected from a long flight during transit over an area far from any sources. 41

3.4 Statistical analysis summary for the counts found in each energy bin for the background measurements collected across the Cambridge-Boston area, listed by date of collection. Maps of the corresponding routes can be found in figure 2-1. 41

3.5 Statistical analysis summary for the counts found in each energy bin for the experiment in the MIT laboratory with a $0.14 \pm 0.07\,\mu Ci$ ^{60}Co source. 41

3.6 Statistical analysis summary for the counts found in each energy bin for measurements from the MIT laboratory with a $3.46\,\mu Ci$ ^{137}Cs source. 42

3.7 Alarm rates from the MIT laboratory with a $3.46\,\mu Ci$ ^{137}Cs source. . 43

3.8 Alarm rates for the experiment in the MIT laboratory with a $0.14 \pm 0.07\,\mu Ci$ ^{60}Co source. 44

3.9 False alarm rates for the UAV flights measuring background at various locations. The background data from Utah was not a dedicated background flight, but data selected from a long flight during transit over an area far from any sources. 44

3.10 False alarm rates for the background measurements collected across the Cambridge-Boston area, listed by date of collection. Maps of the corresponding routes can be found in figure 2-1. 44

Chapter 1

Introduction

The goal of this thesis is to analyze potential solutions to the issue of determining if a radiation source has been found when conducting aerial radiation search and mapping using a drone. Radiation mapping is a process to find anomalous sources of radiation which elevate the count rate above typical background levels. It is an important part of nuclear security as a tool in responding to nuclear disasters in order to find the hazardous areas. Finding a radiation source using an unmanned aerial vehicle (UAV) guided by the radiation detector it is carrying is more complicated because of the changing background radiation, and the speed the drone flies at. The research was done supporting a project at The Charles Stark Draper Laboratory, Inc. to integrate a UAV, radiation/chemical detector, and sensor driven mapping algorithm to map both radiation and chemical hazards. The flight motion of the UAV is directed by the sensor driven contour mapping algorithm developed by The Charles Stark Draper Laboratory, Inc., part of this algorithm is a radiation alarm which the radiation detector updates each second with the spectra and count rate measurements. This alarm takes values of 1 or 0 to indicate that there is or is not an external source of radiation above background present at that time. The purpose of this research is to find the optimal method for the UAV to decide this alarm value given the data it is collecting from the radiation detector.

1.1 Radiation Mapping

The purpose of this thesis is to test alarm methods for use in radiation mapping. Detecting radiaton anomalies involves finding a suspected but unknown radiation source or sources in an area and determining where the radiation hot-spots are. Radiation mapping is an important part of the response to nuclear disasters and can be used to find the fallout. It can also be used in response to potential radiation or nuclear based attacks. This mapping typically produces a visual representation of radiation data from the detector on a map. These maps are an effective and easy to use tool to visualize the distribution of radiation in the contaminated areas, and therefore see which areas are unsafe. Separating signal from background is an important part of radiation mapping, and this is the central challenge of this research. This is also the topic of other radiation mapping research. An example would be recent research done at Berkley using a truck carrying 24 HPGe detectors and a 10x10 array of 10 cm x 10 cm x 5 cm sodium iodide detectors, driving around the San Francisco Bay area. It was found that the background noise was greater and more spread out than noise predicted by Poisson statistics, and a simple first order background estimate was used to overcome this. It was also found that detection rates could be improved significantly by using a linear interpolation for the estimate, and even better performance was found when using measured background data to train the model and fit the coefficients [1].

There are several different platforms that can be used for radiation mapping, each with different advantages and disadvantages. These platforms include cars or vans which have a high payload capacity and power supply and can therefore carry large detectors, but are limited to roads or other light terrain which is easy to drive in [2]. This is what the group at Berkley used and the van had the capacity to carry more and larger detectors than what could be used in this research. However it also meant the areas they were operating in were different than most of the locations where the UAVs could be tested. Detectors can also be carried by people, which can access places vehicles can not but puts the operators at increased risk [2]. Manned aircraft

can cover very large search areas and move fast, but usually fly at higher altitude and the crew can still be put at risk if the radiation levels in the contaminated area are high [2]. The safest way to map radiation is to use unmanned vehicles, since the operators can stay a safe distance away from the area. UAV's can also cover relatively large areas, though not typically as large as larger manned aircraft, and can fly closer to the ground where the radioactive contamination is expected to deposit. The radiation mapping platform selected for the autonomous radiation mapping in this project was a UAV.

1.1.1 UAV Radiation Mapping

As stated previously, the primary advantage of using a UAV for radiation mapping is safety since people do not need to go into an area with dangerous levels of radiation. Some other advantages include the speed and maneuverability of small UAVs and their ability to fly closer to the ground than conventional manned aircraft [2]. However, there are a few disadvantages of using a UAV for radiation mapping. One of the most important current limiting factors on UAVs is battery life. Batteries are heavy and have a limited supply of power, so the endurance and range of UAVs can be very limited compared to ground vehicles, human carried detectors, or conventional aircraft. The UAV used for testing in this project had approximately 20 minutes of battery life; or approximately enough to transit 3 km then search a 1 km^2 area, complete the mission, and return. If the UAV does not need to return it can transit 6 km, search, then land in place. UAVs also have limited payload capacity, which limits the weight of the detector. The detector used in this project has a 45 cm^3 crystal, weighing about 2 lbs. Most of the UAV test flights have been between 10 to 30 of altitude, because of the solid angle the radiation counts fall with distance squared so detector efficiency is important to get enough data. A visual representation of example radiation mapping missions can be found in figure 1-1.

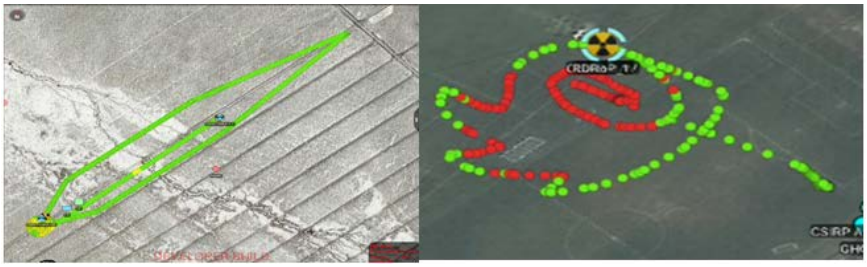

Figure 1-1: Aerial UAV Radiation Mapping. Including a mapping mission with 2 UAVs searchign an area over 1 km away (left). The other is a smaller scale mapping test at Briggs Field at MIT in which the contour pattern is more easily visible (right). Both using real radiation sources of 7.8 mCi ^{137}Cs (right) and a mixed source totalling approximately 98 mCi of mostly ^{60}Co (left).

1.2 Background Radiation

There is always radiation in any given location from natural and celestial sources. Most background radiation encountered in this scenario comes from Naturally Occurring Radioactive Material (NORM). Some of the most common and well known examples of NORM are the uranium and thorium isotopes, products of their decay chains such as radon, and potassium-40. Background radiation is location dependent, both the count rate and the relative fractions of the sources that make up the background radiation spectrum can change. Some common examples of background radiation changing by location are elevated background count rates near buildings because concrete contains small amounts of uranium, or reduced count rates over bodies of water.

1.2.1 Radiation Sources of Interest

In addition to understanding the background radiation, it is also crucial to understand the radiation sources which are being mapped and how they differ from background radiation. This thesis will focus on a few select isotopes that could be of importance during a nuclear disaster or attack scenario. ^{60}Co is an isotope that emits two relatively high energy gamma rays on nearly every decay, which makes it a useful isotope for industrial and research uses. This also means that ^{60}Co could be a plausible contaminant from industrial accidents. It could also possibly be used for a crudely made

radiological dispersal device (RDD), also known as a 'dirty bomb'. Another isotope of interest is ^{137}Cs, which is a daughter product of a common fission product of ^{235}U. This cesium isotope emits a 662 keV gamma. This isotope contributes greatly to the activity of waste from nuclear reactors. It was widely spread over Eastern and Northern Europe during the Chernobyl disaster, contributing greatly to the environmental and health impacts. Another important fission product and component of fallout is ^{131}I, this isotope is a particularly concerning component of fallout because of its biological properties which lead to thyroid cancer. The EPA's list of monitored isotopes related to nuclear weapons testing include both ^{137}Cs and ^{131}I, but also ^{241}Am and ^{90}Sr [3]. For the purpose of UAV radiation mapping the americium and strontium isotopes will be difficult to find because at distances of 10 or more meters the low energy gamma and beta radiation will not stand out much from background. The mean free path of beta radiation is much less than the minimum altitude a UAV would reasonably fly at during a search mission. For this reason, americium and strontium are not among the list of isotopes this thesis will focus on.

1.3 Radiation Detection

1.3.1 CLLBC Detector

All of the experimentation done for this project used a $Cs_2LiLa(Br,Cl)_6$, or CLLBC, scintillation detector from Radiation Monitoring Devices, Inc. (RMD). The crystal volume of the CLLBC detector used in this project is 45 cm^3. CLLBC detectors also have significantly higher resolution compared to other scintillators such as sodium iodide detectors, they can achieve better than 3.5 % full width at half maximum (FWHM) at 662 keV [4]. The density is 4 g/cm^3, which is more dense than typical sodium iodide scintillators. This higher density helps to stop more radiation but the CLLBC is also still lightweight enough for the UAV [4]. The scintillation light output is also relatively high at 45 000 photons/MeV, and the detector typically registers in the range of 9 to 15 cps/µR/h [4]. This translates to background count rates of

approximately 100 to 150 cps in most locations where data was collected for this research. RMD uses an array of silcon photomultiplier (SiPM) to collect scintillation light for further weight reduction.

This detector was selected for the project because of the advantages it provides. It can detect both gamma and neutron radiation while also having higher light output and resolution than most other scintillation detectors. The most important constraints that influence the choice in radiation detectors are the weight limit for the UAV and the limited collection time while moving. While the UAV is mapping radiation counts and a full spectrum are recorded every second and this data drives the search algorithm. A 1 second long measurement has limited counts and statistics so it important the detector be sensitive and high resolution. Since this detector has high energy resolution and sensitivity for a scintillator, there are more counts in the peaks of the energy spectrum so gamma spectroscopy can be used to determine isotope data. The entire detector assembly which attaches to the UAV weighs approximately 3 pounds.

1.3.2 Counting Statistics

A common and simple method of a radiation alarm is to use the statistical properties of radioactive decay with the measured counts. Even in a specific area for a time short relative to the half life of sources where the radiation may be considered "constant", radiation is still a random process and inherent fluctuations will be seen in the data. Radioactive decay, and therefore the count rate recorded by a detector follows a Poisson distribution.

The Poisson distribution is a special case of the binomial distribution described by equation 1.1. In the Poisson distribution the probability of success can be modelled as constant and small [5]. In radiation detection this equation describes the probability of observing a specific number of counts during a measurement.

$$P(x) = \frac{\bar{x}^x \times e^{-x}}{x!} \tag{1.1}$$

An important property of the Poisson distribution is that the standard deviation and mean are related by 1.2.

$$\sigma^2 = \bar{x} \tag{1.2}$$

This property is useful for experiments because it allows for easy calculations of the error on count rates when detecting radiation.

Also important is the central limit theorem. This theorem can be applied to further simplify the Poisson distribution when the mean is sufficiently large. A typical rule of thumb for sufficiently large is greater than 30[5]. The central limit theorem applies to any sequence of independent identically distributed random variables with a common finite mean and variance[6]. The theorem states the convergence to a standard normal cumulative density function (CDF) for Z_n which is defined in terms of n random variables $X_1, X_2, ...X_n$, the mean μ and standard deviation σ by equation 1.3[6].

$$Z_n = \frac{X_1 + ... + X_n - n \times \mu}{\sigma \times \sqrt{n}} \tag{1.3}$$

By definition, a Poisson distribution describes a sum of independent binomial random variables. Therefore if the number of counts is sufficient, then the number of counts detected is described by a Poisson distribution which the central limit theorem also applies to. This means a standard normal CDF can also be applied, which simplifies calculations for the probability of finding a number of counts above or below a specified number of standard deviations from the mean. This allows the use of standard normal tables for probability calculations and the well known rule of thumb that in a normal distribution there is 68 % probability of being within 1 standard deviation of the mean, 95 % for 2 and 99.7 % for 3 standard deviations. When the central limit theorem applies to a sum of independent identically distributed random variables, the sum can be treated as what is called a normal approximation, applied to the Poisson distribution this would be a normal approximation to the Poisson distribution[6].

Assuming the data follows a normal distribution or normal approximation as established by the central limit theorem, a Chi-squared test can be performed. The point of this test is to determine if multiple measurements have fluctuation consis-

tent with the expected distribution[5]. The Chi-squared parameter, χ^2, is defined by equation 1.4.

$$\chi^2 = \frac{1}{\bar{x}_e} \sum_{i=1}^{N} (x_i - \bar{x}_e)^2 \tag{1.4}$$

The reduced Chi-squared parameter, defined as χ^2 divided by the degrees of freedom and can be calculated as the ratio of the sample variance to the mean, can indicate the data has either too much or too little fluctuation to be from the same Poisson distribution. If the value is not close to or less than 1 then it does not match a normal approximation to the Poisson distribution well[5]. The χ^2 value and the degrees of freedom can also be used to calculate the p value. The p value indicates the probability that a random sample from a true normal approximation to the Poisson distribution would result in a larger χ^2 value than the value calculated from the data[5].

When these properties are applied to measured radiation counts or count rates, it allows for easy use of statistics as a radiation alarm. If a measurement is several standard deviations above the previously measured mean count rate in a fixed area, then it is reasonable to conclude that some external radiation source has entered the area. In practice this limit is typically set at 3 or 5 standard deviations. This is a simple, yet powerful tool for stationary radiation monitoring. However it can be problematic for radiation mapping over large areas because it relies on certain assumptions that are not necessarily true when the detector is moving. The use of this simple statistical alarm relies on the assumption of constant mean background count rate. This assumption is most likely invalid for most realistic search areas, and the Chi squared test can be used with moving background measurements to prove so. Background radiation is dependent on the environment and can be higher or lower in some areas. It could be possible for the UAV to have a false negative in an area of lower background, or report false positives in an area of higher background than the location it had previously been moving through.

Receiver Operating Characteristic Curves

The receiver operating characteristic curve (ROC curve) is another concept that is important to radiation detection and related to statistics. The ROC curve characterizes the performance of a detection system by plotting the relationship between the probability of detecting a relatively weak source and the probability of a false alarm caused by statistical fluctuations in the background count rate[5]. A well performing detection and alarm system will have a ROC curve that sharply increases before hitting an inflection point as close as possible towards the point (1,0) then flattens out, with an area under the curve as close as possible to 1. It is physically impossible to get an area under the ROC curve of 1. However the are under the curve can be used to compare real systems, an area under the ROC curve of closer to 1 indicates a better detection system.

1.3.3 GADRAS

Gamma Detector Response and Analysis Software (GADRAS) from Sandia National Laboratory (SNL) has functions that can be used in a radiation mapping scenario as an alarm. GADRAS isotope ID algorithm can be used for isotope identification and confidences from an input spectra. The GADRAS function rate-not-norm can also be used to track the count rate above what is estimated to be background from NORM[7]. GADRAS isotope ID algorithm is an example of gamma ray spectroscopy, in which energy information in the spectrum collected by the detector is used to determine information about the gamma source. This algorithm determines which isotope(s) match the collected spectra and outputs a numerical confidence indicating how strong the spectra fits. The GADRAS Stuff-of-Interest (SOI) function was specifically designed as a radiation search alarm, and has a preset list of isotopes to search for which can be toggled by the user. SOI returns a value ranging from 0 to 10, with values of 3 or more indicating a reasonable level of confidence that a radiation source above background is present[7]. The level of confidence increases with the SOI value.

GADRAS can also be used to create computed spectra of a desired source with a specified detector[8]. Along with some other modelling and simulation capability. Computed source spectra can be useful when there is no real source of a radionuclide to measure in the lab or field.

Chapter 2

Methods

2.1 Data Collection

Developing and determining the efficacy of a radiation alarm requires a large amount of radiation data to be collected. Both background data and data with radiation sources were required. The background data was necessary to characterize typical NORM and to determine the probability of a false positive alarm, or a type I error in statistical terms. The data with radiation sources was used to create the alarm decision criteria for the presence of an anomalous radiation source, and also to determine the type II error rates, or false negative alarms.

2.1.1 Background Measurements

As a standard practice radiation background was measured at the location before most flight tests and the small scale laboratory experiment. The background count rates and energy spectra are important information for a few purposes. This data is necessary to fully analyze the data collected with a radiation source present. This background data is also helpful in measuring the performance of the radiation alarm algorithm. Using the background data can help to find performance metrics such as the type I error rate, how many counts above background the alarm is triggered at, etc.. It is also important to have background measurements from a wide variety of

locations to ensure that the algorithm will work in different locations regardless of the different NORM isotopic abundances encountered in different areas of the world.

In addition to the flight testing locations listed in section 2.1.3, background measurements were also taken in a basement laboratory at MIT, in an apartment in Cambridge, and while moving through the cities of Boston and Cambridge as described in section 2.1.2. Overall the background collection spanned a wide variety of terrain including open fields, forested areas, desert, and urban environments. The background data also comes from 3 different states, including Utah. This is useful since the dose rates from terrestrial radiation can vary widely from location to location and the Rocky Mountain region has some of the highest background in the North American continent [9].

Urban Environment Background

Additional background measurements were done throughout the Boston and Cambridge area. The motivation for these measurements was twofold: longer background collections while moving were helpful to get accurate type I error rates since the flights were typically less than 15 minutes and the only long background measurements were static; also it was desired to have background data from a more complex environment with more fluctuation in the background count rate. As will be explained later in the results section, some of the flight test sites were too small and uniform to see noticeable changes in the background radiation within the search area. One of the critical goals of the alarm algorithm is for it to work in a large area search up to $1\,\mathrm{km}^2$ and to minimize the negative impact of changing background count rates as the detector moves.

These measurements were done on three dates: the 14th, 17th, and 20th of September 2021. The measurements on the 14th and 17th were taken while walking. On the 14th the detector and computer were carried by hand, while on the 17th the detector and computer were carried in a backpack. The measurement on the 20th was done with the detector and computer in a backpack while on a bicycle. All three background measurement routes are depicted in figure 2-1. In total these measure-

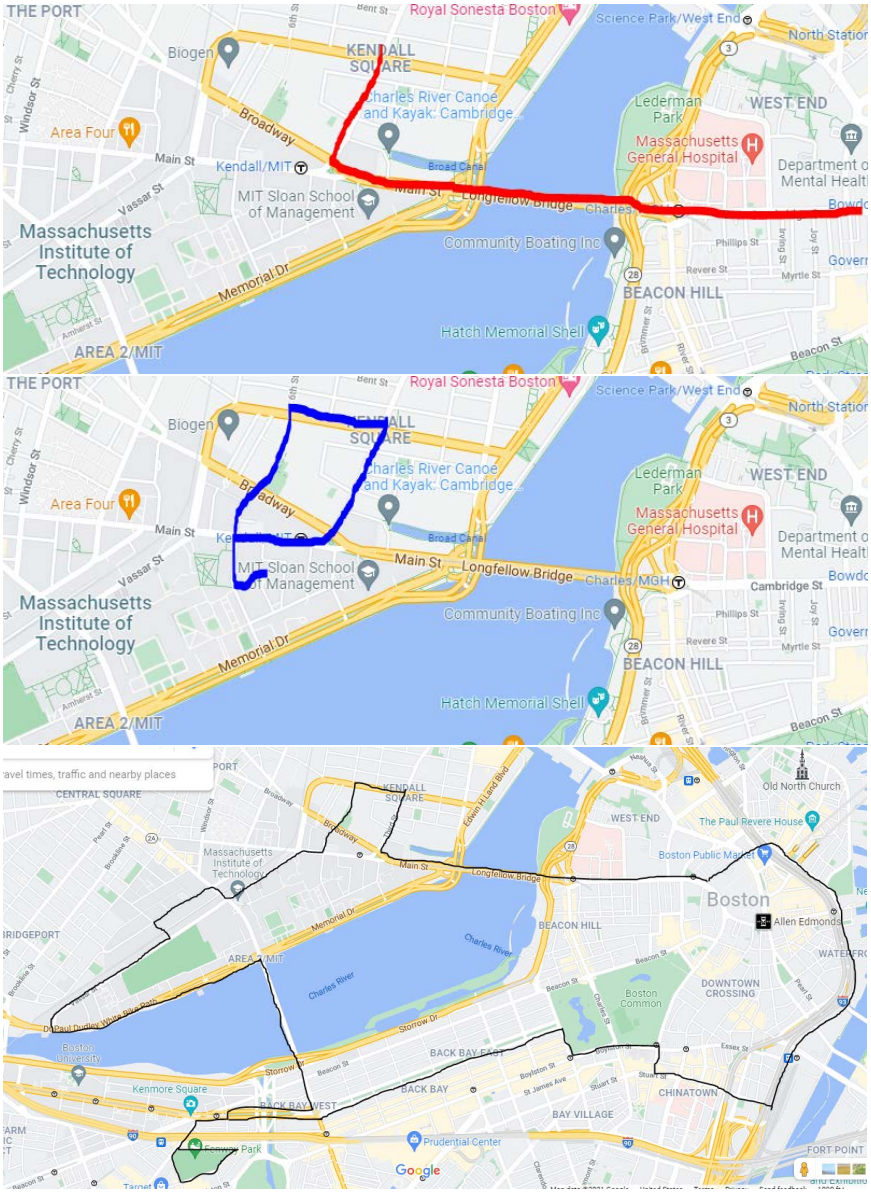

Figure 2-1: Maps of the routes taken through Cambridge and Boston for the background radiation measurements. In order from the 9/14/2021 measurement (top) to the 9/20/2021 measurement (bottom).

ments provided an additional 3 h 5 min 17 s of background radiation data. The routes went over some areas of higher radiation such as near hospitals and construction, and areas of lower radiation such as bridges over water. The route taken on the 20th also passed the MIT research reactor but no elevated count rates were observed in the vicinity.

2.1.2 Laboratory Experimentation

Experimentation was done in a laboratory setting to provide radiation data for the design of the alarm in addition to the flight testing. This was done in order to have more precise and controlled detection conditions than what is possible during flight testing. In a laboratory, distances from source to detector can be measured and controlled more easily than when flying a UAV carrying the detector. The distance also remains constant through the entire measurement while UAVs can drift while hovering. Also battery is not an issue so the time for the measurements is less constrained. Two separate experiments were done in the laboratory with small scale sources, one for ^{137}Cs and one for ^{60}Co. The ^{137}Cs experiment started on December 15th 2021 when a background measurement of approximately 2 h 8 min was taken on the table in the NW14-069 basement lab where the detector would be placed for all subsequent measurements. Data collection also took place on December 16th, 17th, 20th, and the final measurements on January 6th 2022.

The materials used for this were the CLLBC detector, a linux computer to run the ROS commands to operate the detector and record data, a measuring tape, a thin metal table, a chair, and a ^{137}Cs source. The cesium source was reported as 5 µCi in January 2006, according to the exponential properties of radioactive decay and the 30.07 half life of ^{137}Cs the source was approximately 3.46 µCi during these measurements. The source was placed on the chair so that it could be at a similar height to the detector and the chair could be moved to position the source at various distances from the detector. The chair where the source was placed was 2.25 in lower than the table the detector was placed on. Measurements were taken ranging from directly underneath the detector to a 30 in horizontal distance between the source

and detector. The total distance from source to detector for each trial can be seen in either table 3.7 or 3.6 in the results section.

The ^{60}Co experiment took place on March 9th of 2022. It used the same materials in a similar setup however the vertical distance between detector and source was changed to 2.75 in from the previous setup. This testing began with a 20 min background collection followed by three 10 min trials with the source present. The ^{60}Co source was labelled as 0.933 µCi. The source was not labelled with a date but an estimate based on the count rate, geometry, and detector efficiency gave an activity of 0.14±0.07 µCi. The three trials were done at vertical distances of 4 in, 6.5 in, and 1.5 in between source and detector in that order. For this isotope the total distance from source to detector for each trial can be seen in either table 3.8 or 3.5 in the results section.

2.1.3 Flight Testing

Flight testing locations where radiation data was recorded include Briggs Field on MIT campus in Cambridge, Massachussetts; a softball field near Laurel, Maryland; a clearing in a wooded area at Olin College of Engineering in Needham, Massachusetts; Texas; and a high altitude dessert in Utah. A wide variety of radiation sources were used in these tests. The MIT testing used two ^{137}Cs sources with activities of 7.8 mCi and 7.6 mCi, and a 73 mCi ^{241}Am source. The flight test in Maryland used a 85 mCi ^{60}Co source. The testing in Texas used 26 mCi and 8 mCi ^{137}Cs sources. The sources in Utah included: 73 mCi ^{60}Co, 21 mCi ^{60}Co, 0.5 mCi ^{60}Co, a mixed 0.12 mCi ^{60}Co and 1.7 mCi ^{137}Cs source, ten ^{137}Cs check sources totalling 0.9 mCi, two ^{133}Ba sources of 0.3 mCi and 0.29 mCi, 0.18 mCi ^{252}Cf, and 19 mCi depleted uranium. The smaller sources were not strong enough to be seen individually at the altitude the UAV flew at so they were all placed together or with the two large ^{60}Co sources. The flight testing at Olin was only background radiation, no other sources were used. Examples of some of the maps generated during flight tests can be seen in 1-1.

The ^{137}Cs, ^{133}Ba, and ^{241}Am sources are the most useful for determining the function of the alarm in a fallout or nuclear waste scenario. Although the barium

sources were small and both barium and americium are more difficult to detect when flying because of their decay methods as described in section 1.2.1. However, the ^{60}Co sources were also consistently detected and could be a plausible contaminant in a radiation dispersion device or industrial accident.

2.2 Data Analysis

2.2.1 Chi Squared Test For Poisson Distribution

An important assumption in the process creating some of the alarm methods was that traditional Poisson counting statistics were not valid for solving this problem because there would be more fluctuation in background count rates while moving across the search area. It is assumed that Poisson statistics should only be valid in a stationary location with no changes to the radiation sources present during the measurement. However, it is important to test this assumption with data. The Chi Squared test as described in section 1.3.2 by equation 1.4 was applied to both moving background data and data from the lab experiment. The goal of performing the Chi squared test was to verify that the assumption of the count rate being a normal approximation to a Poisson distribution was valid for the count rate in a static controlled environment but invalid when the UAV is performing a realistic radiation mapping mission. The reduced Chi-squared parameter was calculated for simplicity.

2.2.2 Spectra Data and Plotting

The spectra data is recorded from the detector by a ROS (Robot Operating System) code developed by engineers at The Charles Stark Draper Laboratory, Inc. to allow the UAV computer to communicate with both the detector and the flight controller. The data is initially recorded in a rosbag format, the rosbag message containing the spectra data can then be wrote into a comma-seperated values (csv) file format to be more easily handled using a computer with Windows operating system. A series of various python scripts were written to read the spectra data from these csv files,

perform analysis, and write pertinent output files.

One python script was created to read the spectra data from the csv in the original format and reformat the data to write a file following the N42 file format standard. This was necessary for collaboration between The Charles Stark Draper Laboratory, Inc. and Sandia National Labs so that the data was in a format used at Sandia. The N42 file format also allowed the use of GADRAS to plot spectra and count rate time histories from collected data, GADRAS was used to produce many of these plots. However, the plots related to the alarm methods and spectra plots displaying the energy bin setup were created in python.

2.2.3 ROC Curves

ROC curves were generated from the detector data. This was done in python by reading the spectra data from two excel files, one was a background measurement and the other was a measurement with a specific source at a certain distance. Both the files were from the same location for each ROC curve generated. A loop was used to iterate through thresholds to generate a false alarm rate from the background data and probability of detection from the radiation source data. These rates are calculated by finding the proportion of all one second measurement windows which fell above or below the threshold in both files respectively. The false alarm rate and probability of detection for each threshold make up the points that were used to plot the ROC curves. The integrals of the ROC curves were approximated using a trapezoidal sum numerical approach with the data points used to plot the curves. The results of the ROC curves and areas under the curves were used to optimize the alarm methods and thresholds.

An additional complication needed to be addressed when creating ROC curves from flight data. During the flight testing the distance between the source and detector changes rapidly, unlike in a stationary laboratory environment. However, to make a proper ROC curve the data used to make it must have the same source in the same location. Within the same data file from flight testing the source is the same and only the distance to the source changes. To resolve this a check was added to the

python coding so that when generating the probability of detection and false alarm rates, only the measurements taken within a tolerance of a specified input distance would be used. This gives a collection of data points which are approximately the same distance to the source to use to create the ROC curve. The distance data was calculated in python using the Pythagorean theorem with three inputs: GPS data taken by the GPS on the UAV when in flight, GPS location of the source recorded when the tests were set up, and altitude data from the UAV.

2.2.4 Energy Bin and Alarm Methodology

Analysis of the spectra data from the flight testing done in April of 2021 in Texas lead to the use of energy bins to analyze spectra data and an alarm method based on that. The idea was to take advantage of the differences in the energy spectrum of typical background and the sources used in flight testing. NORM and ^{60}Co or ^{137}Cs clearly have very different energy spectra, the goal was to find those differences in a 1 second measurement. A typical spectra from a 1 s measurement has very limited counts in each channel, making it difficult to distinguish peaks and other features important to gamma spectroscopy. Statistical analysis techniques can be used to overcome this challenge and find the small differences in the spectra data. The initial idea was to divide the spectra into 8 energy bins which were all an equal number of channels wide.

This model of 8 energy bins each 128 channels wide was a starting point for developing other alarm methods based on energy bins because it was simple, easy to implement, and also gave a reliable indication of whether a flight had an anomalous radiation source. The bins were made wide since in a 1 second measurement the number of counts in any specific channel is typically very small. A count rate for each bin was found by summing the counts in every channel. The data was then analyzed both by number of counts in each bin and also the proportion of the total counts in each bin. A visual depiction of what the division of the spectra into these 8 bins can be seen in 2-2. The alarm was created from the results of statistical analysis on the energy bins. Two different alarm methods based on the energy bins

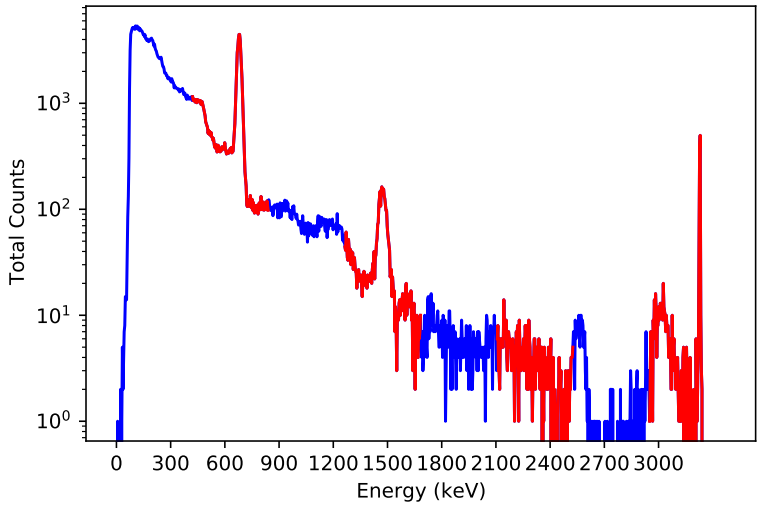

Figure 2-2: Energy spectrum displaying the division of the spectrum into 8 bins, the alternating red and blue regions are the bins. This spectrum data comes from a 30 minute measurement of a 3.46 µCi ^{137}Cs source at a distance of 18.7 cm.

were attempted. The first relies on the fraction of total counts found in the lowest energy bin. Below a certain threshold percentage, the alarm is triggered to indicate the detection of an anomalous radiation source. The second method uses the total counts in each of the bins beyond the lowest energy bin. This was done assuming that counts in these higher energy bins would be less likely to come from background because of observations in the data. Counts above a certain threshold in a bin that is not the lowest energy bin trigger the alarm.

It was recognized that the 8 energy bin alarm method was overly simplistic and not optimized to solve the problem of detecting the isotopes of interest. In an attempt to take advantage of knowledge about the isotopes, a new method was created by reducing the number of bins to 2 and centering the bins around the full energy peaks of the gamma rays emitted by ^{60}Co or ^{137}Cs. These were selected as the primary isotopes of interest for reasons explained in section 1.2.1, but also because all of the measurements used either of the two isotopes. Based on the typical energy calibration of the detector and the resolution, capturing the full peak reliably within the bins required the cesium bin to be channels 168 to 228 and the cobalt bin to be channels

340 to 440, this can be seen in 2-3. The ^{60}Co bin was set to be wide enough to include both the 1332 keV and 1173 keV peaks. These bin centers approximately translate to the energies for the cesium and cobalt peaks because the gain of the detector is 3372 keV over 1024 channels. The energy calibration has slight deviations for each measurement but the gain of the detector stays the same.

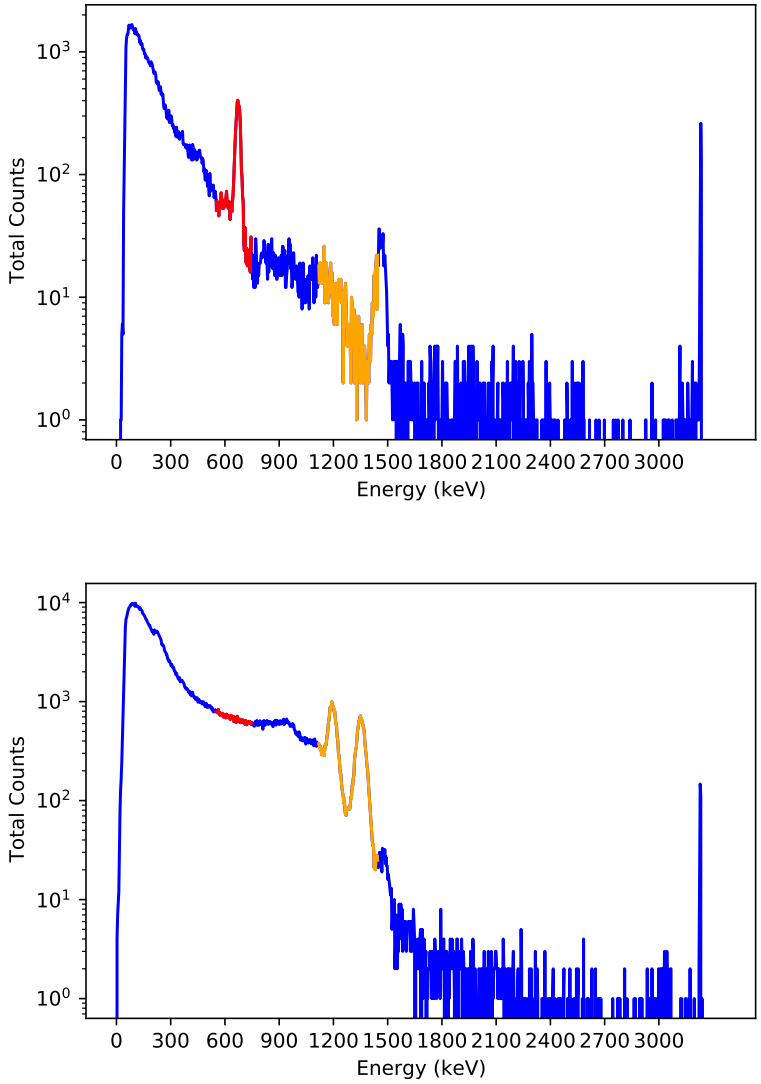

Figure 2-3: Energy spectrum displaying the 2 full peak energy bin setup, the red region is the cesium bin and the orange is the cobalt bin. The spectrum data on the top comes from a flight test with 26 mCi and 8 mCi ^{137}Cs sources, the spectrum on the bottom comes from a flight test with a 85 mCi ^{60}Co. Both flights were at an altitude of 10 m.

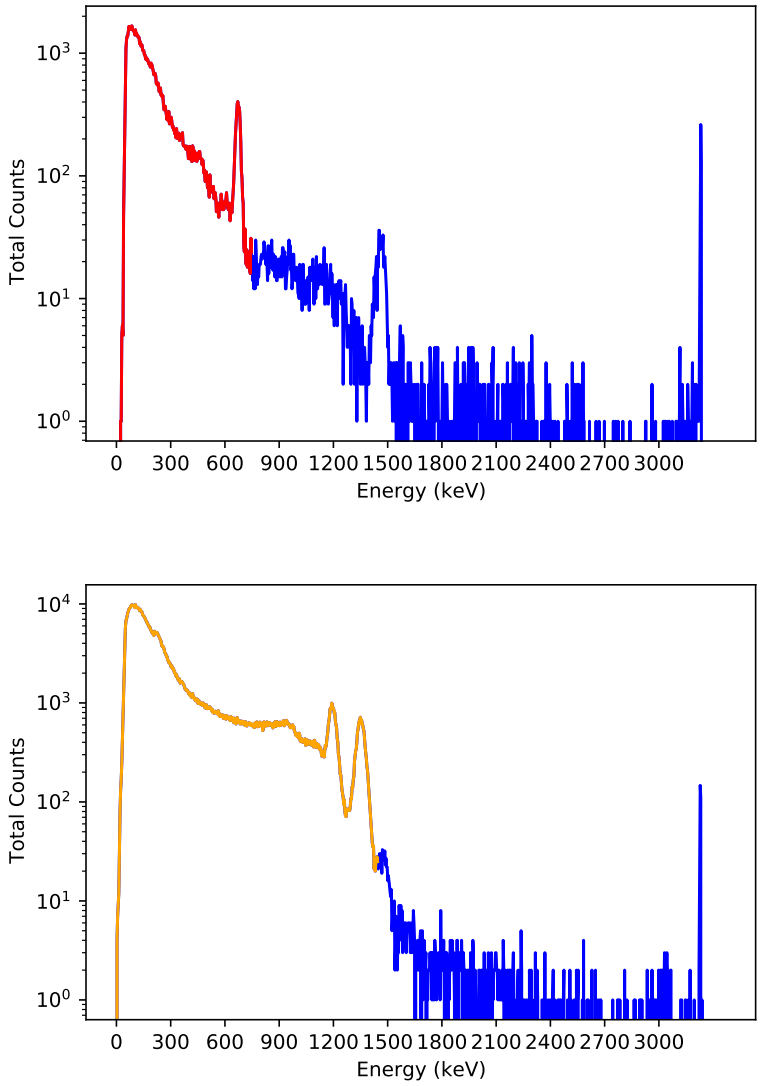

Figure 2-4: Energy spectrum displaying the energy bins from 0 to the full energy peak, the red region is the bin. The top graph displays the cesium bin in red and the second displays the cobalt bin in orange. The spectrum data on the top comes from a flight test with 26 mCi and 8 mCi ^{137}Cs sources, the spectrum on the bottom comes from a flight test with a 85 mCi ^{60}Co. Both flights were at an altitude of 10 m.

One major flaw of the previous 2 bin method is that it only uses a small fraction of the spectra data near the full energy peaks. This would miss other significant features of the spectrum such as the Compton continuum. With the UAV being tens of meters from the source there are non-negligible interactions between the gamma rays and air, meaning more counts will be found in the Compton continuum and less

in the full energy peak. For example at a distance of 50 m only about half of ^{137}Cs gamma rays are completely unattenuated. To address this an additional change to the previous 2 bin method created a third version of the energy bin alarm method. For this version the cesium and cobalt bins were expanded to include the entire Compton continuum and the full energy peak, but none of the high energy background above the full energy peak. For cesium this is channels 0 to 228 and for cobalt channels 0 to 440, this is displayed in 2-4. These three different energy bin alarm methods would be compared to each other and a more basic full spectrum count rate counting statistics approach.

All of the collected data was used to determine the thresholds and to evaluated the performance of the different alarm methods. First, the ROC curves and the area under the curve were used to compare the different methods in the same scenarios in order to determine which alarm method is best. Once the optimal method was selected, the evaluation of performance included the type I error probability and the distance from a known source that the alarm would reliably trigger at. The thresholds were decided after analysis of the ROC curve data.

2.3 Computed Spectra

The isotope ^{131}I was considered to be a possible isotope of interest for the UAV radiation mapping mission because of its abundance in fallout and well known health risks. However, this source was not available for any of the flight testing or the lab experiment. Therefore, computed spectra data from GADRAS was generated for ^{131}I. Simulated data was used to demonstrate how these alarm methods could be applied to iodine or other isotopes of interest. Though the lack of any real flight data means that the performance in a realistic scenario is not as well understood as for ^{60}Co and ^{137}Cs. The majority of analysis was based on collected cesium and cobalt data from flights and the lab. A computed spectra was also made for cesium in order to compare to real data and determine how well the real and computed spectra match. For the iodine spectrum, the bin for the primary full energy peak at 364 keV was channels 100

to 120, the bin containing the Compton continuum and peak was channels 0 to 120. ^{131}I also emits two other gamma energies but the 364 keV gamma is produced over ten times as frequently as the other energies, this peak was also the most prominent in the computed spectra.

Chapter 3

Results

3.1 Chi Squared Test Results

The Chi squared test results are displayed in tables 3.1 and 3.2. The values of the reduced Chi squared parameter indicate that the data collected during the moving urban background testing could not possibly be from the same normal approximation to the Poisson distribution. This fact is even obvious in the large discrepency between the observed standard deviation and the theoretical standard deviation of a Poisson distribution with the observed mean, the measured data had much too high variance. This finding is consistent with what was observed in previous studies such as[1]. This is also seen in the p values which are approximately zero. This was expected, since the background count rate distribution should be changing gradually while moving. Also as expected the data collected during the different trials of the lab experiment and all static background measurements were each found to be consistent with data from a the expected distribution.

The most interesting finding in the results is that some test flights for background radiation were found to not violate the Chi squared test. As seen in table 3.2, two of the flights had p values which would not be statistically significant to reject the null hypothesis, and another flight was close to the borderline case at 0.022. This is assuming the common practice of statistically significant referring to $p < 0.05$. These background flights with higher p values tended to be in small and relatively uniform

Table 3.1: Results of the Chi-squared test for a Poisson distribution for the the background measurements collected across the Cambridge-Boston area, listed by date of collection. Maps of the corresponding routes can be found in figure 2-1. P values below 0.00001 are rounded to 0.

Date	Total Time (s)	Mean	Standard deviation	σ if Poisson	Reduced χ^2	p Value
14-Sep	5071	105	24.98147	10.235263	5.957144576	0
17-Sep	2330	105	23.31467	10.243935	5.179941082	0
20-Sep	3716	103	27.00457	10.126102	7.111969621	0

Table 3.2: Results of the Chi-squared test for a Poisson distribution for various background flights. P values below 0.00001 are rounded to 0.

Location	Total Time (s)	Mean	Standard Deviation	σ if Poisson	Reduced χ^2	p Value
Maryland	443	106	10.78666	10.303739	1.09593449	0.080
MIT 1	81	108	9.896002	10.405957	0.904389465	0.716
MIT 2	140	116	12.07543	10.773314	1.256338077	0.022
Texas	1030	87.5	12.10957	9.352327	1.676556248	0.000
Utah	160	107	12.12256	10.360683	1.369027675	0.001

areas such as the softball field in Maryland, or MIT Briggs Field. The results for these specific flights suggest that the variation found in the data was not too high compared to what would be expected in data from a single normal approximation to the Poisson distribution. This result seems surprising at first since it is expected that the background distribution should be changing as the UAV moves. However, it does make sense for a few reasons. First, these flight testing areas were small, and relatively uniform. The background distribution is unlikely to change much when moving from one end of a soccer field to another. Also in general the changes in background levels are typically very gradual, abrupt sharp changes are usually rare or unnatural. The sharp changes in the urban background seem to be unique to that more challenging and complex environment.

3.2 Bin Analysis and Alarm Results

3.2.1 ROC Curves

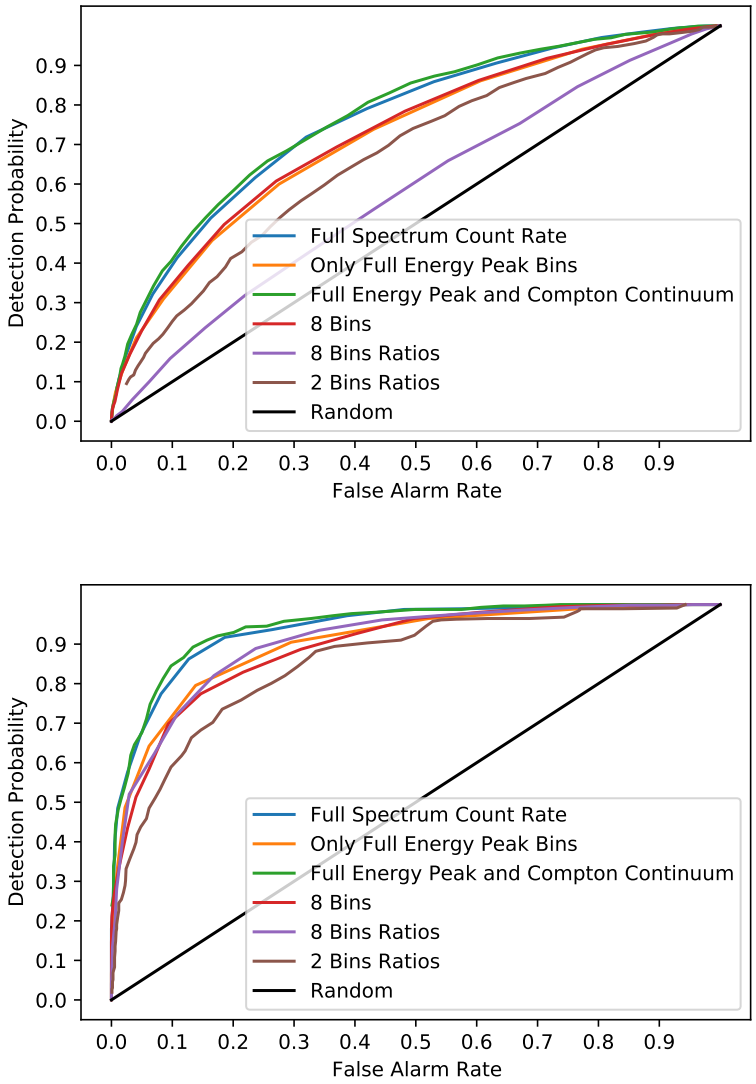

Figure 3-1: ROC curves for all of the alarm methods attempted, and the hypothetical random line for reference. The top ROC curve uses data collected 76.4 cm from a 3.46 µCi ^{137}Cs source. The curve on the bottom was measured 17.9 cm from a 0.14 µCi ^{60}Co source.

The ROC curve analysis indicated that the most sensitive alarm design is to use the two bins from 0 to the full energy peak of the target isotopes of cobalt and cesium. This method maximized the integral under the ROC curve for all curves generated regardless of isotope or location. This is slightly more sensitive than using the full spectrum, which goes approximately from 0 to 3300 keV. This is because high energy background is cut out while retaining all data coming from the cobalt or cesium

source(s). ROC curves from a laboratory environment can be seen in 3-1 and curves made from flight test data can be seen in 3-2. A few extra steps were involved in making the ROC curves from flight test data, and the curves in 3-2 were plotted using only the data points that were collected at a distance of 100±2 m from the source. The two bins capturing only the cesium and cobalt peak energies performed worse, and the gap was wider when using flight data. This makes sense since in the flight testing the distance from the source is much larger, giving more opportunity for attenuation in air which would cause more of the spectrum to be concentrated in the Compton continuum. The eight bin method also had worse performance than the two bins which captured the entire Compton continuum and full energy peak, as expected. Surprisingly the eight bin method had comparable ROC curve results to the two bins capturing only the full energy peak. Thresholds based off ratios of energy bins proved to be inferior to count based thresholds by a significant margin in most cases. The alarm setup with the best ROC curve results will be the focus of the rest of the analysis.

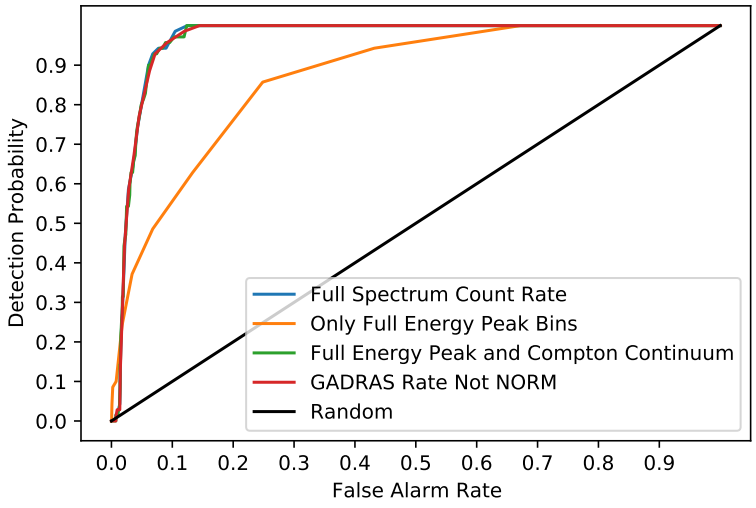

Figure 3-2: ROC curves created from flight test data, only the full spectrum, and 2 bin methods were plotted. The ROC curve uses data collected from a flight at 25 m altitude with several sources placed together totalling approximately 98 mCi of mostly ^{60}Co. The curve was made with data selected to be approximately 110 m from the source.

3.2.2 Type I Error Rates

With the selected alarm method described in the previous section, the type I error rates were determined. This was done by finding the percentage of individual 1 s measurements during the total measurement time during which the alarm was triggered for several background measurements. The threshold selected for this analysis was 3σ over the mean background counts in either bin. The means and standard deviations used for this can be found in 3.3 for several background flights in various locations, and in 3.4 for the urban background measurements. False alarm rates were also calculated for the static lab background measurements, the means and standard deviations for every trial of those two experiments are in 3.5 and 3.6.

Table 3.3: Statistical analysis summary for the counts found in each energy bin for the UAV flights measuring background at various locations. The background data from Utah was not a dedicated background flight, but data selected from a long flight during transit over an area far from any sources.

Location	Cs Bin Mean	Co Bin Mean	Cs Bin Standard Deviation	Co Bin Standard Deviation	Cs Bin 1 Percentile	Co Bin 1 Percentile	Cs Bin 99 percentile	Co Bin 99 percentile
Maryland	97.6	103.1	10.5	10.6	75	78	124	129
MIT 1	100.4	105.8	9.2	9.7	81	86	122	130
MIT 2	107.9	113.1	11.6	11.9	82	85	135	140
Texas	79.3	84.6	11.3	11.8	55	60	105	112
Utah	96.8	103.5	11.2	11.8	73	81	123	130

Table 3.4: Statistical analysis summary for the counts found in each energy bin for the background measurements collected across the Cambridge-Boston area, listed by date of collection. Maps of the corresponding routes can be found in figure 2-1.

Date	Cs Bin Mean	Co Bin Mean	Cs Bin Standard Deviation	Co Bin Standard Deviation	Cs Bin 1 Percentile	Co Bin 1 Percentile	Cs Bin 99 percentile	Co Bin 99 percentile
14-Sep	94.4	101.3	81.0	81.3	41	45	160	172
17-Sep	95.4	102.2	21.8	22.9	62	67	171	181
20-Sep	95.2	102.2	23.4	24.6	49	54	174	184

Table 3.5: Statistical analysis summary for the counts found in each energy bin for the experiment in the MIT laboratory with a $0.14 \pm 0.07\,\mu\text{Ci}$ ^{60}Co source.

Trial	Distance to Source (cm)	Cs Bin Mean	Co Bin Mean	Cs Bin Standard Deviation	Co Bin Standard Deviation	Cs Bin 1 Percentile	Co Bin 1 Percentile	Cs Bin 99 percentile	Co Bin 99 percentile
Background	N/A	116.8	125.5	10.6	11.1	91	99	142	151
1	2.5	150.4	178.7	12.1	13.2	125	150	183	212
2	5.1	132.5	150.9	11.1	12.0	110	123	159	180
3	7.6	183.7	232.5	14.4	16.0	153	197	219	274

Table 3.6: Statistical analysis summary for the counts found in each energy bin for measurements from the MIT laboratory with a 3.46 µCi ^{137}Cs source.

Trial	Distance to Source (cm)	Cs Bin Mean	Co Bin Mean	Cs Bin Standard Deviation	Co Bin Standard Deviation	Cs Bin 1 Percentile	Co Bin 1 Percentile	Cs Bin 99 percentile	Co Bin 99 percentile
Background	N/A	115.5	124.0	10.8	11.2	91	99	142	151
1	5.7	1316.9	1327.9	36.5	36.7	1237	1247	1397	1407
2	5.9	942.2	951.8	29.5	29.6	872	883	1015	1025
3	6.3	757.9	767.0	26.6	26.8	700	709	819	828
4	6.9	631.3	640.1	24.1	24.4	577	586	688	699
5	7.6	557.0	565.7	23.6	23.8	505	513	611	622
6	8.5	470.0	478.6	22.2	22.4	522	532	420	429
7	9.5	407.0	415.6	20.6	20.7	457	466	361	369
8	10.6	378.6	387.0	20.4	20.7	330	338	426	436
9	11.7	338.7	347.2	18.1	18.4	299	306	383	391
10	12.8	306.7	315.5	17.6	18.0	267	274	350	360
11	13.9	279.6	288.3	16.5	16.7	241	249	318	326
12	15.1	263.0	271.8	15.5	15.8	229	237	299	308
13	16.3	245.2	253.9	15.2	15.4	210	220	279	290
14	17.5	232.5	241.2	15.2	15.6	198	205	268	278
15	18.7	217.4	225.9	14.7	14.9	183	192	252	260
16	19.9	211.7	220.4	14.5	14.9	179	188	246	257
17	21.1	198.7	207.5	14.1	14.4	168	176	232	241
18	23.6	188.6	197.5	13.6	14.0	157	164	222	231
19	26.0	175.3	184.1	13.0	13.4	146	154	205	215
20	28.5	167.4	176.1	12.9	13.2	137	146	196	207
21	31.0	161.9	170.7	12.8	13.2	134	142	191	201
22	38.5	148.8	157.6	12.2	12.6	122	130	177	187
23	46.1	140.8	149.7	11.6	11.9	116	124	168	177
24	53.6	134.6	143.3	11.6	12.0	109	117	164	173
25	61.2	132.2	141.0	11.5	11.9	106	113	160	169
26	36.0	153.6	162.2	12.7	13.0	126	133	185	195
27	33.5	157.0	165.6	12.6	12.9	128	135	186	196
28	41.0	143.9	152.9	12.2	12.5	116	124	173	184
29	43.6	142.4	151.2	11.7	12.1	117	124	170	180
30	76.4	127.0	135.8	11.2	11.7	101	109	154	164

The false positive rates, determined as described in the previous paragraph, were very low in the laboratory data. As seen in tables 3.7 and 3.8, the type I error rates for both experiments were in agreement at just over 3 per 1000. The probabilities of false alarm were more inconsistent with flight data, shown in table 3.9. Some flights had no false alarms, some had similar false alarm rates to lab data. Interestingly, two background flights at MIT Briggs field on the same day gave very different false alarm rates. One of the flights had no false alarms while the other appeared to have an exceptionally high false alarm rate of 1.23%, making it an outlier point in the background flight data. An important note is that this flight was only 81 s and there was a single false alarm. A weighted average of both MIT background flights accounting for the different duration of each flight gives a reasonable false alarm rate of 0.45%. The median background flight had a false alarm rate of only 0.19%. Alternatively, the background measurements collected walking and biking across Boston and Cambridge did tend to produce significantly higher false alarm rates than the lab and flight data, and this was not merely a product of short detection times. These false alarm rates are in table 3.10. The higher false alarm rates in the

larger and more complex areas were expected, and are in agreement with the increased variability in background count rates found in the Chi squared test analysis. The September 14th measurement only had a low false alarm rate because of the higher observed standard deviations in the counts in the bins.

Table 3.7: Alarm rates from the MIT laboratory with a 3.46 µCi ^{137}Cs source.

Trial	Distance to Source (cm)	Alarm Rate (%)
Background	N/A	0.33%
1	5.7	100.00%
2	5.9	100.00%
3	6.3	100.00%
4	6.9	100.00%
5	7.6	100.00%
6	8.5	100.00%
7	9.5	100.00%
8	10.6	100.00%
9	11.7	100.00%
10	12.8	100.00%
11	13.9	100.00%
12	15.1	100.00%
13	16.3	100.00%
14	17.5	100.00%
15	18.7	100.00%
16	19.9	100.00%
17	21.1	100.00%
18	23.6	99.89%
19	26.0	98.75%
20	28.5	94.09%
21	31.0	87.80%
22	38.5	56.17%
23	46.1	30.36%
24	53.6	14.99%
25	61.2	10.32%
26	36.0	69.32%
27	33.5	79.44%
28	41.0	39.61%
29	43.6	35.43%
30	76.4	4.27%

Table 3.8: Alarm rates for the experiment in the MIT laboratory with a 0.14±0.07 µCi ^{60}Co source.

Trial	Distance to Source (cm)	Alarm Rate (%)
Background	N/A	0.34%
1	4.9	94.19%
2	7.1	26.28%
3	3.1	100.00%

Table 3.9: False alarm rates for the UAV flights measuring background at various locations. The background data from Utah was not a dedicated background flight, but data selected from a long flight during transit over an area far from any sources.

Location	Alarm Rate (%)
Maryland	0.45%
MIT 1	1.23%
MIT 2	0.00%
Texas	0.19%
Utah	0.00%

Table 3.10: False alarm rates for the background measurements collected across the Cambridge-Boston area, listed by date of collection. Maps of the corresponding routes can be found in figure 2-1.

Date	Alarm Rate (%)
14-Sep	0.05%
17-Sep	1.59%
20-Sep	1.40%

3.2.3 Distance from Source of Alarm

The distances from the radiation source(s) of each 1 s measurement were calculated for several flights using the method described in section 2.2.3. This could not be done for all data files because certain criteria had to be met. The flights for which these distance calculations were made needed: GPS data saved from the flight, altitude data saved in the data files, a recorded GPS location for the radiation source(s), and the rows of GPS data needed to be matched with the rows of spectrum data. Most collected flight data met at least one or a few of these requirements but only eleven flights met all of them. The thresholds used for this were the same as what was used in the false alarm calculations for the same locations. This section will focus on the flight testing data, however in 3.8 and 3.7 reported alarm rates at specified distances

from the lab data are reported. The lab data is more controlled and precise, but less realistic for a UAV radiation mapping mission.

In both flights with the single 85 mCi cobalt source, the alarm was triggered during every second of both flights. This is because of the large source and small area, with the UAV taking off only about 71 m horizontal distance from the source. The maximum total distance between source and detector was 72 m in the first flight and 74 m in the second. The other flights gave more interesting information since the UAV was able to start far enough away from the source to not immediately trigger the alarm. A 1207 s long test flight in Utah using just the 73 mCi Cobalt source was able to still alarm at a nearly 75% rate at distances of over 150 m from the source. This flight also had only one measurement closer than 130 m to the source that did not alarm. Two other flights in Utah used all of the gamma sources piled together totalling approximately 98 mCi of mostly ^{60}Co. In the flight at 15 m altitude the alarm rate was 100% for all data point collected less than 147 m from the source. The flight at 25 m with the same source had a 91% alarm rate in the 70 data points that were 110±2 m from the source. One of the test flights in Texas was done with only the 26 mCi cesium source, the alarm rate was 7 out of 9 for data points between 40 and 52 m from the source and a few alarms were even observed at distances just over 55 m.

Some of the flight were more complicated with sources in multiple locations. This required additional check to ensure that the distances for the alarm values correspond correctly to the source that most likely caused the alarm. For example, if the detector is 30 m away from two sources of relatively equal strength they cannot be easily isolated, but if the detector is 20 m from an 8 mCi source and 100 m from a 15 mCi source it can be assumed which source caused the alarm. This also depends on the relative strength of the sources. In the Texas flights it was found that the probability of detection was over 90% for the 8 mCi cesium source at distances between 20 and 24 m in the setup with the sources most isolated to ensure no overlap. While in the same flight the alarm was successfully triggered for every measurement under 52 m from the larger 26 mCi cesium source. During the test in Utah a few flights were done

with the 73 mCi cobalt source placed 60 m from the 21 mCi cobalt source, then all the smaller sources totalling about 3.8 mCi placed another 60 m further down. The lower altitude UAV was able to achieve an 80% detection rate between 148 to 158 m from the largest source. Neither UAV flew close enough to the smallest source to find it, never coming within 40 m of it. Since the middle source was only 60 m from the largest source and that was well within the range where the largest source could be detected, a detection range for this source could not be separated out of the data. These results support that this alarm method could be sensitive enough for practical use in UAV radiation mapping.

3.3 Computed Spectra Results

Before analysis was done on computed ^{131}I specrtra data, real data was checked against computed data to determine how well the spectra matched. Trial 21 of the cesium experiment, a setup with the source 31 cm from the detector, was used to compare real and computed data. A computed spectrum was created with the same source strength and distance as this measurement, and approximately the same measurement time of around 30 min. The computed and real spectra for the same cesium source at the same distance were significantly different, as seen in figure 3-3. The computed data had a higher count rate and the full energy peak was much higher. This could be due to some differences between the model and real detector setup that give higher detection efficiency in the simulation, such as the plastic casing around the detector or the metal stand the detector was on during data collection. The simulated data does not appear to be interchangeable with the measured data. In this case simulated and real data should not be combined, and simulated data should not be used to estimate real detection distances or false alarm rates.

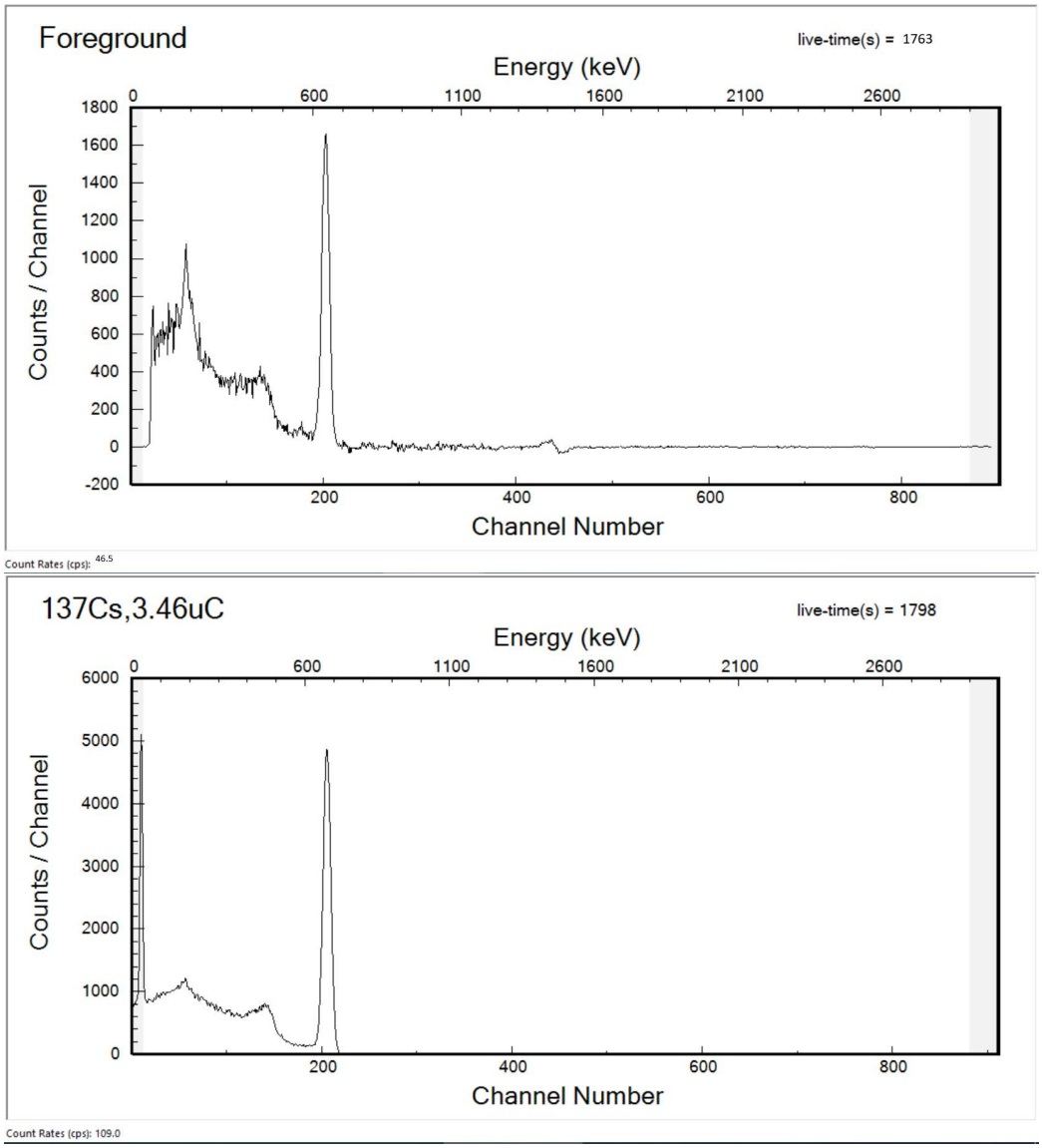

Figure 3-3: Spectra plots with background subtracted for real experimental (top) and computed (bottom) data. Both spectra are approximately 30 min at 31 cm from a 3.46 µCi ^{137}Cs source. Count rates above background and live time for the measurements are in the plots, the y axes are different scales because the simulated data has a much higher 662 keV peak.

However, computed iodine data could still provide evidence that the alarm methods described and analyzed earlier could be applied with other isotopes or even with different detector responses that what was used in the data collection. An ROC curve was made using computed iodine data and computed background data, seen in 3-4. The general observations from this plot were the same as those made from the real

data despite the differences in the spectra data, the best performance came from using the full energy peak and Compton continuum for the isotopes of interest while ignoring higher energy background.

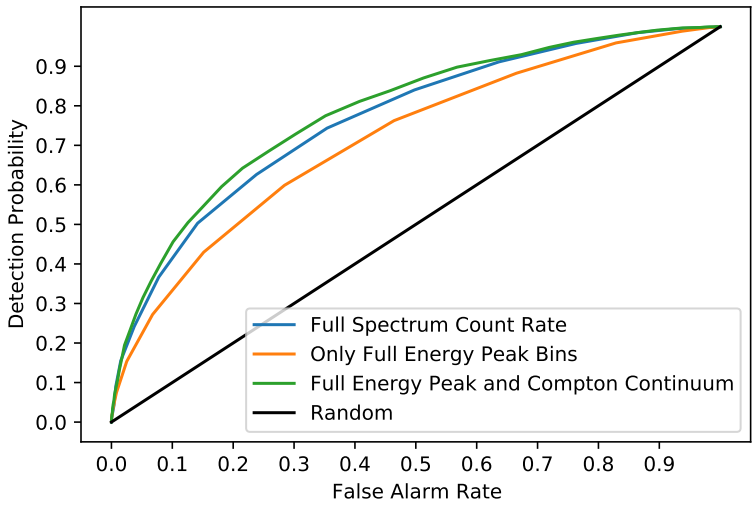

Figure 3-4: ROC curves created from computed data in GADRAS, only the full spectrum, full energy peak bin, and Compton continuum and full energy peak bin were included. The data was simulated as 10 m from a 100 µCi ^{131}I source.

Chapter 4

Conclusions

As stated in the previous section, the most sensitive alarm method tested was to use a bin for each isotope of interest containing all of the spectrum channels up to but not beyond the peak energy. The data suggests that out-performing the sensitivity of using counting statistics with the full spectrum count rate is difficult. The recommended implementation of this would be to begin a radiation mapping mission by collecting background data either while hovering after takeoff or during transit to the search area for at least a minute. Then using a 3σ threshold on the background bins as the alarm for the remainder of the flight. Data analysis earlier in this thesis demonstrates that this method maximizes sensitivity and would work without issue in many UAV radiation mapping scenarios. In five of the six background flights analyzed the false alarm rate is 0.45% or less, translating to only approximately 5 false alarms over a 20 min flight. A flight of that length is approaching the limit of battery life for the UAV's used in this setup. The median background flight false alarm rate of 0.19% translates to only approximately 2 false alarms over a 20 min flight. This method also maximized the area under the ROC curve, meaning it is more sensitive than other methods. Using this method to determine the threshold worked with data from the Utah flight testing, indicating that a prior background collection flight over the search area is not necessary for this to work. The data used as the background from the Utah testing is from an approximately 1 km transit. So this example also supports that this alarm method could still work for large search

areas and long transits to the search area.

However, there are some limits to this approach. Searching in more complex environments such as urban areas could result in significantly increased rates of type I errors, type II errors, or both. There are a few ways to mitigate this issue. It could be accounted for in the mission planning and deployment of radiation mapping UAVs with this alarm method to not be used in cities. Instead it would be better to use a different alarm algorithm for these locations such as one of the GADRAS functions or the background subtracting method described by [1]. Alternatively, the alarm method of energy bins containing only the peak energies of isotopes of interest proved to be much more resistant to changing background levels, although it was less sensitive. Another potential issue is this approach is also relatively simple and basic, although that could also help by reducing the computing power required for the alarm. Also, the method used for this thesis focuses only on a small list of isotopes. While the method could be applied to other isotopes of interest, it does require some assumptions or prior knowledge about what sources are being searched for in order to be most effective. This is not necessarily always a bad assumption, but situations could arise in which this is a disadvantage.

These findings can be useful for radiation mapping using autonomous vehicles, which is an important tool in the response to a nuclear attack or disaster. In the future, more research on the topic could expand the list of isotopes this method has been tested with. Also, since all of the data analysis was done by post processing data of flights, it would be advisable to observe the results of an autonomous flight test using this alarm method before implementing it. However, based on the analysis done so far it can be concluded that this method could have sufficient performance for UAV radiation mapping as is. The simulated data also suggests that this method could work with other isotopes or potentially even other detectors than what was used in the tests done for this research. With additional testing and verification, the alarm method selected in this thesis could be serviceable for practical radiation mapping missions.

Bibliography

[1] Timothy J. Aucott et al. Effects of background on gamma-ray detection for mobile spectroscopy and imaging systems. *IEEE Transactions on Nuclear Science*, 61(2):985–991, April 2014.

[2] Luis Marques, Alberto Vale, and Pedro Vaz. State-of-the-art mobile radiation detection systems for different scenarios. *Sensors*, 21:1051–, February 2021.

[3] Radioactive fallout from nuclear weapons testing, 2021. US Environmental Protection Agency.

[4] CLLBC Gamm-Neutron Scintillator Properties. RMD.

[5] Glenn F. Knoll. *Radiation Detection and Measurement*. John Wiley & Sons, Inc., fourth edition, 2010.

[6] Dimitri P. Bertsekas and John N. Tsitsiklis. *Introduction to Probability*. Athena Scientific, second edition, 2008.

[7] Dean J. Mitchell and Lee Harding. Gadras isotope id user's manual for analysis of gamma-ray measurements and api for linux and android. 2015.

[8] Steven M. Horne, Gregory G Thoreson, Lisa A. Theisen, Dean J. Mitchell, Lee Harding, and Wendy A. Amai. Gadras-drf 18.5 user's manual.

[9] Environmental radiation, 2010. Health Physics Society.